A study of the reproducibility of electron beam induced deposition for sub-20nm lithography

Hari, Sangeetha; Verduin, Thomas; Kruit, Pieter; Hagen, Cornelis W.

DOI
10.1016/j.mne.2019.04.003

Publication date
2019

Document Version
Final published version

Published in
Micro and Nano Engineering

Micro and Nano Engineering 4 (2019) 1–6

Contents lists available at ScienceDirect

Micro and Nano Engineering

journal homepage: www.journals.elsevier.com/micro-and-nano-engineering

Research paper

A study of the reproducibility of electron beam induced deposition for sub-20 nm lithography

Sangeetha Hari, Thomas Verduin, Pieter Kruit, Cornelis W. Hagen*

Department of Imaging Physics, Faculty of Applied Sciences, Delft University of Technology, Lorentzweg 1, 2628CJ Delft, The Netherlands

ARTICLE INFO

Keywords:
Electron beam induced deposition
EBID
Reproducibility
Nano-lithography
Scanning electron microscope

ABSTRACT

The potential of Electron Beam Induced Deposition (EBID) to become a reliable and reproducible direct-write nanopatterning technique has been investigated. A key requirement is that patterns of sub-20 nm dimension can be reproducibly fabricated and measured. EBID was used for the controlled fabrication of sub-20 nm dense lines on bulk silicon. To study the reproducibility of the fabrication process, a method for the quantitative measurement of line widths was developed. The line width of sub-20 nm EBID lines has been determined to be reproducible to within 1 nm. The parameters of importance and the challenges in achieving reproducibility, for performing EBID in standard SEM's, are discussed.

1. Introduction

An important requirement for a lithography technique is that fabricated patterns are reproducible. To judge the reproducibility, metrology is used to measure specific properties such as line width and line edge roughness of patterns consisting of dense lines and spaces. In the semiconductor industry, where resist based lithography is being used, reproducibility is key and metrology techniques such as scatterometry and critical dimension scanning electron microscopy (CD-SEM) are widely used. However, when patterns of sub-10 nm dimension are needed other lithography techniques may become relevant, perhaps as a complementary technique to standard resist-based lithography. To become successful such novel techniques have to be reproducible and reliable metrology techniques have to be available. In this work we address Electron Beam Induced Deposition (EBID) [1–3] and its potential as a reproducible novel lithography technique. EBID is a resist-free nanopatterning technique that is very attractive for high resolution applications due to its ability to fabricate sub-10 nm patterns. EBID is usually carried out in a Scanning Electron Microscope (SEM) by focussing the primary electron beam onto the substrate in the presence of adsorbed precursor gas molecules which have been let in through a nozzle close to the sample surface. The electrons interact with the substrate, generating high energy backscattered and low energy (< 50 eV) secondary electrons, all of which interact with the molecules causing them to dissociate. The non-volatile dissociation fragment forms a deposit on the substrate, and in this manner patterning can be carried out by simply scanning the beam along a predefined path. A major advantage of EBID is the high resolution achievable by the use of a focussed electron beam, which has been demonstrated in numerous reports, from sub-5 nm dots [4,5] to few nanometre wires [6]. Sub-10 nm gaps have been fabricated in devices [7–10] using EBID directly, as a mask, or in combination with a metallic layer to enable specific functionality. Due to the versatility of EBID, it has been used for several applications such as the fabrication of electrodes, etch masks, nanorods, 3-dimensional, plasmonic and even superconducting nanostructures [11,12]. Another great advantage is in the inherent ease of use and flexibility. A variety of materials can be deposited by the use of appropriate precursors [2] and being an inherently 3D technique, it also enables the growth of structures in height. It requires no resist or sample preparation. In addition, there are few restrictions on the substrate to be patterned, accommodating in principle everything from flat wafers to spherical and uneven surfaces. Extensive reviews of EBID and EBIE can be found in [2,13–15]. These properties make EBID potentially very attractive for high resolution lithography.

So far, there have been no studies on the reproducibility of EBID, nor can this be deduced from a survey of EBID experiments in literature. This stems mainly from a lack of understanding of the patterning regime in these experiments. The study of reproducibility requires knowledge, or at least maintenance, of patterning conditions and parameters. This is often difficult to achieve due to factors like precursor diffusion and local gas flux, which are hard to control. As described in [16] this problem can be overcome by patterning in the electron current limited regime where variations in precursor-related parameters are less significant and the reproducibility, by extension,

* Corresponding author.
E-mail address: c.w.hagen@tudelft.nl (C.W. Hagen).

https://doi.org/10.1016/j.mne.2019.04.003
Received 12 October 2018; Received in revised form 11 March 2019; Accepted 7 April 2019

would be expected to be higher. This work demonstrates lithography by EBID in the electron current limited regime. The deposition is controlled by controlling the beam parameters and the sensitivity of deposit dimensions to the remaining parameters is measured. This includes, among others, fluctuations in beam current and temperature, drift, vibrations, varying chamber contamination levels, surface inhomogeneities and accuracy of beam positioning.

The next important issue in the determination of reproducibility is the metrology of dense EBID lines. This has hardly been discussed in literature. Cross sections of EBID lines are typically not rectangular shapes but rather Gaussian shapes, requiring new methods to obtain reliable line edge positions and line widths. Most often in EBID, deposits on bulk substrates are imaged using Secondary Electron (SE) detection and/or Atomic Force Microscopy (AFM), from which the dimensions are determined simply by inspection. This is obviously not a robust technique and cannot be used for comparing images, especially at the sub-20 nm scale. Moreover, the interpretation of the SE contrast of EBID lines is not straightforward due to effects like enhanced SE emission from the sloped sidewalls [17,18] In conclusion it is safe to say that there is almost no data available on the reproducibility of high resolution dense EBID lines, the first report being as recent as 2014 [16]. Here we present the first systematic study of the reproducibility of sub-20 nm dense EBID lines, fabricated under regular circumstances in a standard electron microscope.

2. Methods

A Thermo Fisher Nova Nano Lab 650 Dual Beam system was used for EBID, and patterning was carried out using an in-house Labview program which positioned the beam as per coordinates defined in a stream file. Patterning was performed within an area of approximately 1 mm^2 of the silicon substrate. Multiple data sets were acquired over an interval of about a year. When a stage move of 100 µm or more was performed between repetitions of the pattern, the beam focus was verified before resuming patterning. This was performed by focusing on markers adjacent to the patterning field comprising nanosized grains of gold-palladium. A part of the layout of a chip is shown in the left image in Fig. 1. The circles visible are fields of silicon covered with native oxide, meant for patterning. The labels A2, A3, etc. are also made of silicon. The rest of the chip is covered with a layer of gold-palladium (about 30 nm thick), so that the edges of the fields (indicated by the red square in the left image) as shown in the high magnification image on the right act as markers for focussing the beam. The patterning field itself was not scanned prior to the fabrication of the lines, in order to avoid contamination.

Lines were patterned in the horizontal as well as vertical direction, mainly to see the effect of possible drift or bias with respect to the nozzle or detectors. They were patterned in both serial and parallel mode with serpentine writing strategy. The SEM chamber was vented and pumped down a few times in between, each time to a base pressure in the range 2×10^{-6} mbar to 5×10^{-6} mbar, so the effect of varying contamination levels, if present, could be noted. The sample was always mounted at eucentric height and placed in the same orientation with respect to the door of the SEM. The Gas Injection System (GIS) temperature was maintained at 45 °C, and the gas load was 1.2×10^{-5} mbar. The nozzle of the GIS was aligned at the very beginning to be 150 µm above the sample at eucentric height and 75 µm away from the centre of the field of view, and no special efforts were made to maintain this alignment over time. Patterning was begun 45 min after the GIS temperature had reached the set value. After an hour or so of patterning, the GIS valve was closed, the needle retracted and the heater switched off for an hour, before repeating the inlet procedure for the next set of deposits. On one occasion, the chamber was cleaned using an oxygen plasma overnight prior to patterning the next morning. On the others, no special efforts were made to clean the system. It should be noted that during this period, the SEM was also used for other (unrelated) EBID work, involving use of the same precursor and a variety of samples. The idea of this scheme was to take into account the sensitivity of the process to real-life patterning circumstances where the GIS, for example, is not always realigned prior to patterning, nor is the contamination level of the chamber necessarily the same during all experiments. The sample was stored in a clean wafer box before being loaded into the SEM. It was not subjected to any cleaning procedure.

All sets of lines were imaged on a Thermo Fisher Verios 460 SEM in Ultra High Resolution (UHR) mode simultaneously with the two in-column backscattered electron (BSE) detectors: In Column Detector (ICD) and Mirror Detector (MD). In this mode, the sample is immersed in a magnetic field, resulting in a smaller spot size and therefore higher resolution. BSE's having different emission angles and energies are focussed differently, resulting in different signal intensities at the ICD and MD. The imaging conditions were: working distance of 4 mm, beam energy of 5 keV, beam current of 50 pA and resolution of 1536 by 1024 pixels. The pixel dwell time and the detector settings are parameters that could be quite critical in obtaining a good image. A higher dwell time could improve the image quality by increasing the signal to noise ratio, but it could also lead to increased sample contamination by EBID, thereby worsening it. The detector contrast and brightness, which can be varied independently on a scale of 0 to 100, determine the grayscale values in the image, and to enable proper information capture and comparison between images, a protocol must be devised to set the right values. The imaging strategy and the influence of these parameters on the measurement of line width were investigated systematically and optimised for use in this work.

The edge detection technique used was an improved version of the technique described in [16]. The integrated intensity profile of the set of EBID lines was plotted and any background slope present in it was subtracted. The plot was smoothed and a function was fitted. Due to the different base levels adjacent to different EBID lines, a normalised double Gaussian function, vertically shifted and matched at the centre was used. The fit was performed by allowing all the parameters to vary. Then this function was fitted to each scan line of each EBID line

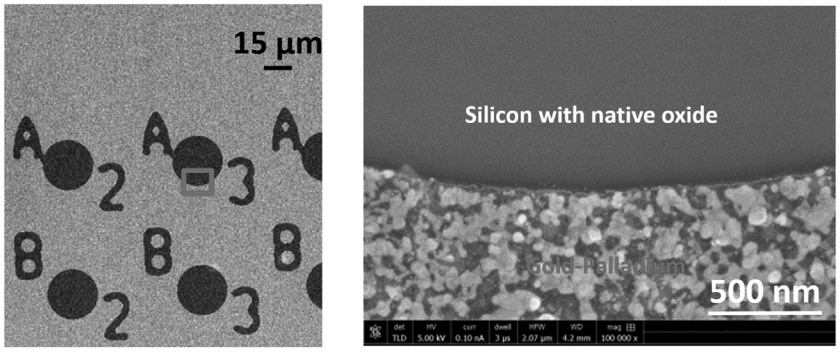

Fig. 1. Layout of the chip used for patterning. Left: The circles are fields of silicon covered with native oxide, meant for patterning. The labels A2, A3, etc. are also made of silicon. The rest of the chip is covered with a layer of gold-palladium (about 30 nm thick), so that the edges of the fields (indicated by the red square in the left image) can be used for focussing the beam. Right: High magnification image of the region indicated by the red square, showing the nanoscale grains of gold-palladium that were used for focusing the electron beam. (For interpretation of the references to colour in this figure legend, the reader is referred to the web version of this article.)

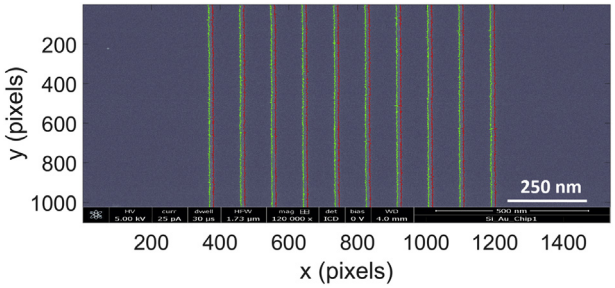

Fig. 2. An example case, showing the edges of the EBID lines (in red and green) plotted on an ICD image of 10 nm wide dense lines of Set - 1a (Conversion: 1 pixel = 1.1 nm). (For interpretation of the references to colour in this figure legend, the reader is referred to the web version of this article.)

Table 1
Two sets of dense EBID lines patterned for the study of reproducibility. Set-1a and Set-2a were patterned with defined line widths 10 nm and 15 nm respectively, at a centre-to-centre spacing of 100 nm, and repeated after one year (Set-1b and Set-2b).

Set	1a	1b	2a	2b
Defined width	10 nm	10 nm	15 nm	15 nm
Line spacing	100 nm	100 nm	100 nm	100 nm

allowing only lateral translation of the double Gaussian function. The centre position was thus determined for each scan line and a straight line fit through these points was used to determine the centre of the EBID line. Next, with the centre positions fixed, the same function was fitted to each scan line, this time allowing the width of the double Gaussian function to vary. The edge positions, defined as the 1σ distance from the centre on either side, were determined from this fit, as well as the line width (LW) defined as the distance between the left and right edge. An example is shown in Fig. 2 where the edges of the lines are indicated in red and green.

Table 2
Mean line widths of each line in a typical image of Set-1a, determined using edge detection.

Line	Mean line width
Line 1	14.2 nm
Line 2	14.3 nm
Line 3	14.5 nm
Line 4	14.2 nm
Line 5	14.3 nm
Line 6	14.0 nm
Line 7	14.2 nm
Line 8	14.0 nm
Line 9	14.2 nm
Line 10	14.1 nm

Table 3
Mean line widths of the lines of Set-1a imaged using the ICD and MD.

Set	Mean (LW-Set)	Std
Set – 1a: 10 nm horizontal lines (ICD images)	15.7 nm	0.3 nm
Set – 1a: 10 nm vertical lines (ICD images)	14.2 nm	0.9 nm
Set – 1a: 10 nm horizontal lines (MD images)	15.2 nm	0.3 nm
Set – 1a: 10 nm vertical lines (MD images)	13.9 nm	1.0 nm

3. Results and discussion

Two sets of high resolution dense EBID lines (Set-1a and Set-2a) were patterned with defined widths of 10 nm and 15 nm respectively, with a centre to centre spacing of 100 nm, as described in Table 1. Each set, comprising 10 vertical and 10 horizontal lines, was repeated several times (minimum 5 and maximum 20) over approximately 1 mm^2 of the sample. The patterning was performed on a silicon chip with a layer of natural oxide by EBID from the organometallic precursor $MeCpPtMe_3$. The lines were patterned with a dose of 400 C/m^2 using a 20 keV, 40 pA beam. The estimated spot size at these settings is 1.6 nm. A patterning pitch of 1 nm (along the length and width of the line) and pixel dwell time of 1 μs were used. The patterning strategy for each line was

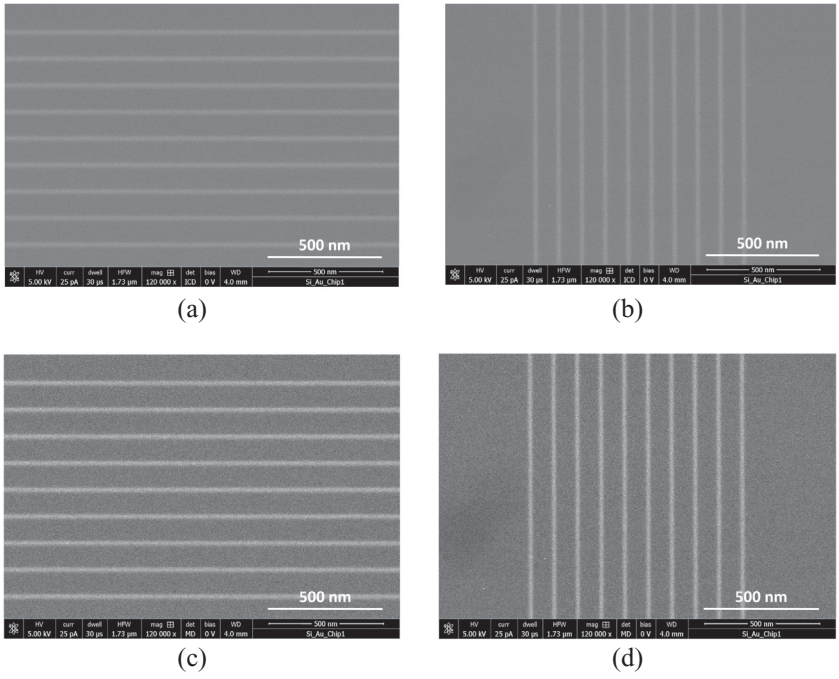

Fig. 3. Typical images of the dense lines of Set-1a (a) ICD images of 10 nm wide horizontal lines (b) ICD images of 10 nm wide vertical lines (c) MD images of 10 nm wide horizontal lines (d) MD images of 10 nm wide vertical lines.

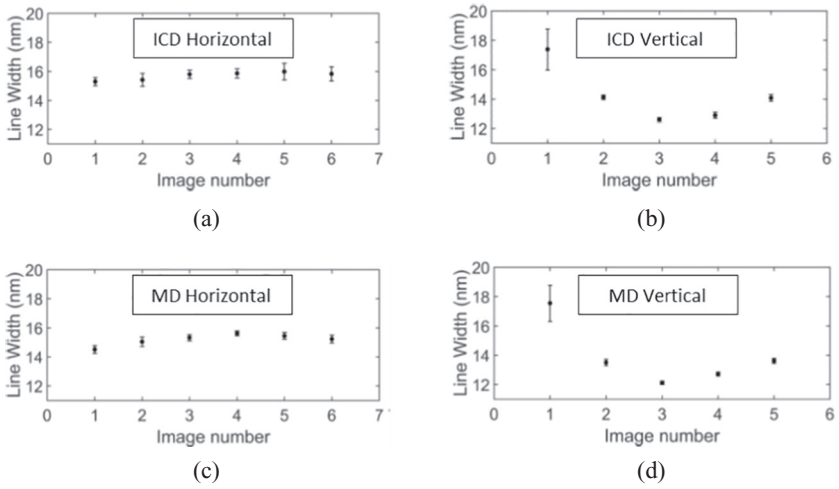

Fig. 4. Plots showing the reproducibility of LW in Set 1a for (a) ICD images of 10 nm horizontal lines (b) ICD images of 10 nm vertical lines (c) MD images of 10 nm horizontal lines (d) MD images of 10 nm vertical lines.

Table 4
Mean line widths of the horizontal and vertical lines of Set – 1b, Set – 2a and Set – 2b measured from ICD and MD images.

Set	Mean (LW-Set)	Std
Set - 1b: 10 nm horizontal lines (ICD images)	21.5 nm	1.6 nm
Set - 1b: 10 nm vertical lines (ICD images)	16.8 nm	0.6 nm
Set – 2a: 15 nm horizontal lines (ICD images)	23.5 nm	< 0.1 nm
Set – 2a: 15 nm vertical lines (ICD images)	19.8 nm	0.1 nm
Set – 2a: 15 nm horizontal lines (MD images)	23.2 nm	0.1 nm
Set – 2a: 15 nm vertical lines (MD images)	18.9 nm	0.1 nm
Set - 2b: 15 nm horizontal lines (ICD images)	27.6 nm	3.1 nm
Set - 2b: 15 nm vertical lines (ICD images)	20.0 nm	0.6 nm

serpentine and the desired dose was delivered in 10 passes. The patterning was repeated after one year (Set-1b and Set-2b respectively) on the same system with the same beam parameters. These parameters were chosen to ensure patterning in the electron current limited regime [16], and this was further verified by the patterning of test structures to ascertain the absence of diffusion-induced proximity effects. The reproducibility is therefore also expected to be higher in this regime. Homogeneous deposits were obtained, which were then repeated as described in the Methods section, for the measurement of reproducibility.

We aim to characterize the lines as is performed in resist-based lithography, i.e., by the measurement of line width (LW). The lines were imaged simultaneously with the two different in-column backscattered electron detectors: MD and ICD, in the UHR mode in a Thermo Fisher Verios 460 SEM. Typical images of Set-1a are shown in Fig. 3.

The line widths were measured using the edge detection technique described in the Methods section, and the mean width of each line was determined as shown in Table 2. This analysis was performed for every image, and yielded the mean resultant width of lines defined 10 nm and 15 nm wide.

The mean line width = mean (LW-Set), defined as the average over 1σ values of line width from the MD and ICD images of the set, is shown in Table 3 and the results of this analysis performed over all the images of Set -1a is shown in Fig. 4 as the scatter in LW over the set. The scatter in the line width observed in the above plots gives a measure of the reproducibility of high resolution patterning by EBID. The error bars in the reproducibility plots of the different sets are the standard deviation in 1σ LW within an image, i.e., over 10 lines.

The mean line widths of Set – 1b, Set – 2a and Set – 2b were determined similarly and the values are shown in Table 4. Imaging was performed with both the backscattered detectors wherever possible, but due to sustained problems with the MD in the latter half of the experiments, only ICD images could be acquired for Set – 1b and Set – 2b.

Since the patterning and imaging conditions for lines within an image and within a set were the same, the variation in LW across a set is an indication of the sensitivity of EBID to ambient conditions and the statistics of the process. We define reproducibility as the standard deviation of LW over the set: Reproducibility = std.(LW-Set). The width of a new line patterned under identical conditions can therefore be predicted to be: LW-New = mean (LW-Set) ± std.(LW-Set). The data

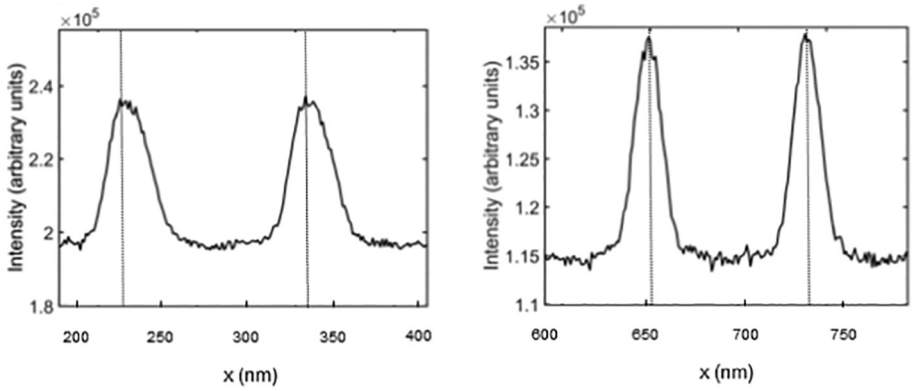

Fig. 5. Plot comparing the line profiles of horizontal and vertical lines from ICD images. The dotted lines at the position of the peak intensity show the asymmetry in the case of the former.

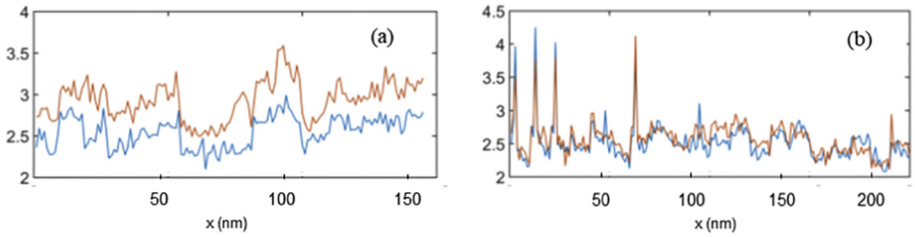

Fig. 6. Plot of the standard deviation of the left and right edges for the (a) horizontal and (b) vertical lines of Set-1b (from ICD images), averaged per line, clearly showing that the edges are correlated, likely as a result of the presence of vibrations in both directions.

Table 5
Reproducibility of EBID lines of each set.

Set	Type	Reproducibility
1a	Vertical	0.9 nm
1b	Vertical	0.6 nm
2a	Vertical	0.1 nm
2b	Vertical	0.6 nm
1a	Horizontal	0.3 nm
1b	Horizontal	1.6 nm
2a	Horizontal	< 0.1 nm
2b	Horizontal	3.1 nm

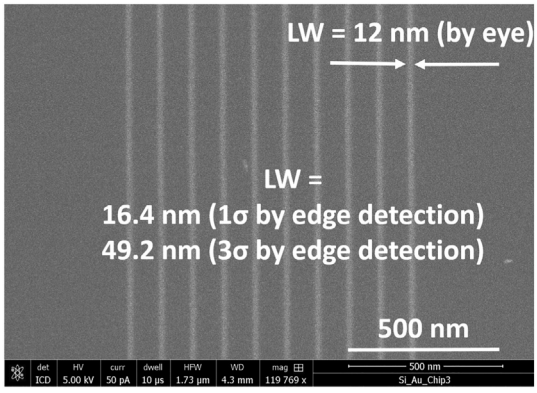

Fig. 7. An SE image of dense EBID lines that appear 12 nm wide upon measurement by eye. Edge detection reveals the 1σ value of LW to be 16.4 nm and the 3σ value to be 49.2 nm, attesting to the necessity of accurate metrology in high resolution EBID.

above show a spread in LW for 10 nm and the 15 nm lines over time and there appears to be a significant difference between horizontal and vertical lines. The width of vertical lines is on average lower than that of identically defined horizontal lines. Since the order of patterning within a field was: 10 nm horizontal lines, 10 nm vertical lines, 15 nm horizontal lines, and finally 15 nm vertical lines, this could not be attributed to loss of beam focus. But it could possibly be explained by drift or vibrations. The patterning time per line was in the range of 10 ms, from which we can deduce that if the broadening came about due to drift, it must be about 1000 nm/s, which is unrealistically high (a typical value for the system is 0.2 nm/s). It might be due to vibrations that have a larger amplitude in one direction. It must be noted that the same observation holds for lines patterned a year later on this microscope (Thermo Fisher Nova Nano Lab 650). Also, no significant difference in LW of horizontal and vertical lines was observed while patterning on the Verios 460 SEM. So it is most likely due to stage vibrations in the system. If that is the case, the vibrations must have occurred during patterning because the Verios 460 SEM was used for imaging of all the sets. The horizontal lines are also seen to have a highly asymmetric profile compared to the vertical lines of the same set from inspection of the integrated SEM profiles. For the example case from Set-1b presented in Fig. 5, the mean position of the left edge is 9.1 nm from the centre and that of the right edge is 13.0 nm, for the horizontal lines. For the vertical lines, the numbers are 9.2 nm and 9.9 nm respectively, much lower in comparison. This also supports the idea that there were effects interfering with the patterning.

In another test, several sets of lines were selected from the experiments and the plot of the standard deviation of the left and right edges shown in Fig. 6 shows that the edges are correlated. This is true in the case of both horizontal and vertical lines, and suggests the presence of vibrations in both directions, which could have been present during patterning or imaging or both.

The reproducibility of the EBID lines of each set is shown in Table 5. The reproducibility of vertical lines is within 1 nm and that of horizontal lines is within 3 nm. These values are very low, which is promising for high resolution patterning. It should be kept in mind, however, that reproducibility of a set has been defined as the scatter in LW within the set of lines patterned, and it is not, for example, a physical quantity like the line edge roughness. The inherent reproducibility of high resolution EBID patterning can therefore be as good as 1 nm. The lower reproducibility observed in the patterning of horizontal lines may be due to the stage vibrations that also led to the asymmetric line profiles observed.

The reliability of patterning over time emerges from a comparison of Set 1 (1a and 1b) and Set 2 (2a and 2b) which were patterned with a gap of approximately one year. In this time, although changes such as refilling and realigning the GIS and major repair work including replacement of the pole piece and remounting of the stage had taken place, it is reassuring to see that the maintenance of identical beam parameters during patterning is sufficient to ensure reproducibility in the process. A comparison of the mean LW of vertical lines of Set-1a and Set-1b as well as Set-2a and-2b shows differences of less than 1 nm.

The LW determined from simultaneously acquired ICD and MD images is the same to within approximately 1 nm. Although the LW from the MD images is consistently lower, this difference falls within the error of the measurement and is not significant. For the study of reproducibility, either detector can be used to image the lines.

4. Conclusions

Sub-20 nm dense EBID lines have been fabricated in the SEM using the standard platinum precursor $MeCpPtMe_3$. The line width has been measured for several sets of lines of different defined widths, using a newly developed edge detection technique, providing quantitative 2D characterisation of dense EBID lines.

Most often in literature, the dimensions of EBID deposits are measured merely by eye, meaning that the dimensions in the SEM image are measured using the scale bar provided by the imaging software and by user definition of the two points between which to measure. This is entirely insufficient for high resolution patterns. The lines shown in Fig. 7, for example, appear to be about 12 nm wide when measured by eye. But an accurate measurement performed by edge fitting reveals the 1σ value of LW to be 16.4 nm. The error in the measurement by eye is about 4 nm; in other words, the measured value is about 37% higher than it appears to be by visual inspection, which is quite significant. The

3σ value, therefore, containing almost the entire extent of the line, is 49.2 nm. Moreover, for electrical measurements where it is important to know the extent of the deposited material that is conducting, the 3σ value is perhaps more relevant, in which case the error is huge. Metrology of EBID lines is therefore crucial at high resolution. In fact, even for large deposits, depending on the application, it may be unwise to report numbers by eye as that amounts to ignoring the shallow deposit present in the tails of the pattern.

The reproducibility of sub-20 nm dense EBID lines patterned in the electron current limited regime has been measured and found to be very high. The line width is reproducible to within 1 nm. Varying contamination levels, gradual GIS misalignment (over a year), small variations in gas load, fluctuations in temperature, variations in diffusion rates and surface roughness of the silicon sample have been found to not affect the deposited line width by more than 1 nm. This is reassuring because it means that these parameters, which are difficult to measure, do not in fact need to be monitored if standard working conditions are maintained.

Some sample orientations with respect to the stage seem to result in broader and more diffuse deposits, possibly due to vibrations. If it is not possible to take steps to reduce the vibrations in the system, it is important to take this directional dependence into account prior to patterning. Failure to do so would lead to loss of resolution and reproducibility.

Author contributions

The manuscript was written through contributions of all authors. All authors have given approval to the final version of the manuscript.

Notes

The authors declare no competing financial interests.

Declaration of Competing Interest

None.

Acknowledgment

The authors acknowledge funding from NanoNextNL. This work was conducted within the framework of the COST Action CM1301 (CELINA).

References

[1] A. Botman, J.J.L. Mulders, C.W. Hagen, Creating pure nanostructures from electron-beam-induced deposition using purification techniques: a technology perspective, Nanotechnology 20 (37) (Sep. 2009) 372001.
[2] I. Utke, P. Hoffmann, J. Melngailis, Gas-assisted focused electron beam and ion beam processing and fabrication, J. Vac. Sci. Technol. B Microelectron. Nanom. Struct. 26 (4) (2008) 1197.
[3] M. Huth, et al., Focused electron beam induced deposition: a perspective, Beilstein J. Nanotechnol. 3 (Jan. 2012) 597–619.
[4] W.F. van Dorp, B. van Someren, C.W. Hagen, P. Kruit, P.A. Crozier, Approaching the resolution limit of nanometer-scale electron beam-induced deposition, Nano Lett. 5 (7) (Jul. 2005) 1303–1307.
[5] W.F. van Dorp, B. van Someren, C.W. Hagen, P. Kruit, P.A. Crozier, Statistical variation analysis of sub-5-nm-sized electron-beam-induced deposits, J. Vac. Sci. Technol. B 24 (2) (2006) 618–622.
[6] N. Silvis-Cividjian, C.W. Hagen, P. Kruit, M.A.J. v. d. Stam, H.B. Groen, Direct fabrication of nanowires in an electron microscope, Appl. Phys. Lett. 82 (20) (2003) 3514.
[7] A.N. Broers, W.W. Molzen, J.J. Cuomo, N.D. Wittels, Electron-beam fabrication of 80-Å metal structures, Appl. Phys. Lett. 29 (9) (1976) 596.
[8] C.T.H. Heerkens, M.J. Kamerbeek, W.F. van Dorp, C.W. Hagen, J. Hoekstra, Electron beam induced deposited etch masks, Microelectron. Eng. 86 (4–6) (Apr. 2009) 961–964.
[9] A. Bezryadin, Nanofabrication of electrodes with sub-5 nm spacing for transport experiments on single molecules and metal clusters, J. Vac. Sci. Technol. B Microelectron. Nanom. Struct. 15 (4) (1997) 793.
[10] I.G.C. Weppelman, P.C. Post, C.T.H. Heerkens, C.W. Hagen, J.P. Hoogenboom, Fabrication of narrow-gap nanostructures using electron-beam induced deposition etch masks, Microelectron. Eng. 153 (2016) 77–82.
[11] S. Sengupta, et al., Superconducting nanowires by electron-beam-induced deposition, Appl. Phys. Lett. 106 (4) (2015) 042601.
[12] M. Winhold, P.M. Weirich, C.H. Schwalb, M. Huth, Superconductivity and metallic behavior in $Pb_xC_yO_8$ structures prepared by focused electron beam induced deposition, Appl. Phys. Lett. 105 (16) (2014) 162603.
[13] W.F. van Dorp, C.W. Hagen, A critical literature review of focused electron beam induced deposition, J. Appl. Phys. 104 (8) (2008) 081301.
[14] S.J. Randolph, J.D. Fowlkes, P.D. Rack, Focused, nanoscale electron-beam-induced deposition and etching, Crit. Rev. Solid State Mater. Sci. 31 (3) (Sep. 2006) 55–89.
[15] N. Silvis-Cividjian, C.W. Hagen, "Electron beam–induced nanometer-scale deposition", advances in imaging and electron, Physics 143 (6) (2006) 1–235.
[16] S. Hari, C.W. Hagen, T. Verduin, P. Kruit, Size and shape control of sub-20 nm patterns fabricated using focused electron beam-induced processing, J. Micro/Nanolithography, MEMS, MOEMS 13 (3) (Jul. 2014) 033002.
[17] L. Reimer, Scanning Electron Microscopy, Vol. 45 Springer, Berlin, Heidelberg, 1998 No. 9.
[18] H. Hiroshima, Fabrication of conductive wires by electron-beam-induced deposition, Nanotechnology 9 (1998) 108–112.